International Journal of Fatigue 31 (2009) 2006–2013

Contents lists available at ScienceDirect

International Journal of Fatigue

journal homepage: www.elsevier.com/locate/ijfatigue

Microcrack growth and fatigue behavior of a duplex stainless steel

M. Balbi [a], M. Avalos [a], A. El Bartali [b], I. Alvarez-Armas [b,*]

[a] Instituto de Física Rosario, CONICET – Universidad Nacional de Rosario, Bv. 27 de Febrero 210 bis, 2000 Rosario, Argentina
[b] Laboratoire de Mécanique de Lille (LML, UMR CNRS 8107), Ecole Centrale de Lille, BP 48, 59651 Villeneuve d'Ascq Cedex, France

ARTICLE INFO

Article history:
Received 10 September 2008
Received in revised form 10 December 2008
Accepted 16 December 2008
Available online 25 December 2008

Keywords:
Low cycle fatigue
Duplex stainless steel
Microcracks
Microstructure
Aging

ABSTRACT

The kinetics of microcrack growth during cycling has been studied in a S32205 duplex stainless steel in the as-received and aged (100 h at 475 °C) conditions. Cylindrical specimens with a shallow notch were subjected to a constant plastic strain range of 0.3% in both thermal conditions. The characteristic features of surface damage and crack growth showed striking differences in microcrack density, nucleation location and propagation rate between the two thermal conditions even though the fatigue lives are comparable. In the as-received material, microcrack density is low and they nucleate mainly at grain and phase boundaries or second-phase particles. In the aged condition, slip markings first appear in the ferritic phase and they are the preferred site for microcrack nucleation. Crack propagation takes place along slip markings in adjacent grains for crack lengths less than 100 μm. A comparison between fatigue life and the relevant parameters of a microcrack growth law was made.

1. Introduction

Duplex stainless steels (DSS) are stainless steels that contain a mixture of ferrite and austenite grains. These steels combine very good mechanical and corrosion properties as compared to single-phase-stainless steels (ferritic or austenitic), making them suitable for the offshore, chemical and power industries [1]. Although DSS are regarded as high-potential industrial materials, they are susceptible to spinodal decomposition when exposed to temperatures between 300 and 500 °C. The decomposition of the ferritic phase leads to higher hardness, yield stress and ultimate tensile strength, but it dramatically decreases ductility and toughness. Although the influence of spinodal decomposition on the mechanical properties of DSS under monotonic loading is well documented, it has been studied much less extensively under cyclic loading. Even fewer investigations have examined the evolution of the surface damage before microcraking begins. Recently, Armas et al. [2,3] have studied the cyclic behavior of DSS of different generations. They found that DIN 1.4460 with no nitrogen content and small amounts of molybdenum suffers from loss of toughness and a pronounced decreasing of the fatigue life when it is fatigued in the aged condition at room temperature. On the other hand, the new generation UNS S32750 (super) duplex stainless steels with much higher nitrogen and molybdenum content has shown comparable fatigue life between the aged and as-received conditions and no loss of toughness in either condition has been observed.

The aim of this work is to study the surface damage evolution in the standard DSS in the as-received and aged conditions and to correlate it with the internal dislocation structure in order to determine the mechanisms of microcrack nucleation and propagation.

2. Experimental procedure

2.1. Material

The material studied in this investigation is the type SAF 2205 DSS supplied by SANDVIK manufactured in the form of hot-rolled and solution annealed cylindrical bars. The chemical composition (in wt. %) is: C: 0.016; Cr: 22.0; Ni: 5.4; Mo: 3.1; N: 0.16; Fe: balance. The structure of the steel was composed of islands of austenite elongated in the rolling direction embedded in a ferritic matrix. The material was studied in two different thermal conditions: as-received (hot-rolled and solution annealed) and aged 475 °C for 100 h. Fig. 1 is the optical micrographs of the etched surface of a section parallel to the bar axis in the as-received form. The volume fraction of austenite is approximately 50% and the average austenitic grain size in the plane perpendicular to the specimen axis is about 10 μm. A careful microstructural analysis showed that the steel is free of intermetallic phases. It is well known that a crystallographic orientation relation exist between austenite (fcc) and ferrite (bcc) in cast duplex stainless steels [4]. Such orientation relations are currently encountered in wrought duplex stainless steels. The most common is the Kurdjumov–Sachs (K–S) relations $\{111\}_\gamma//\{110\}_\alpha$ $[110]_\gamma//[111]_\alpha$.

The principal longitudinal monotonic tensile properties in both thermal conditions are: YS = 550 MPa, UTS = 750 MPa, in the

* Corresponding author. Fax: +54 341 4821772.
E-mail addresses: alvarez@ifir-conicet.gov.ar, alvarez@fceia.unr.edu.ar (I. Alvarez-Armas).

0142-1123/$ - see front matter © 2009 Elsevier Ltd. All rights reserved.
doi:10.1016/j.ijfatigue.2008.12.007

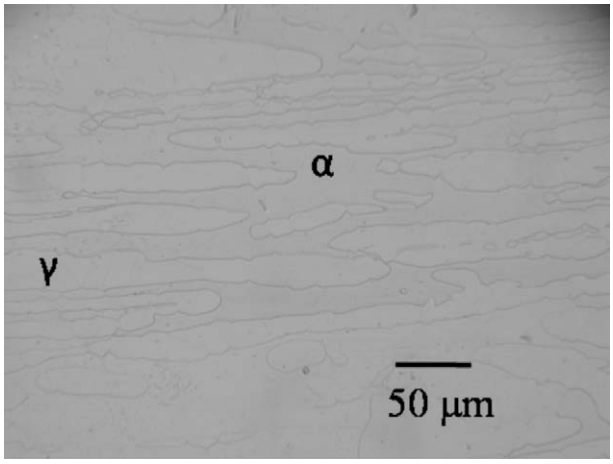

Fig. 1. Optical micrographs from 2s parallel to the tensile axis in the as-received condition in SAF 2205 DSS.

as-received form and YS = 830 MPa, UTS = 953 MPa, in the aged condition. The elongation in the aged condition is reduced in 10% related to the as-received form.

2.2. Test specimen preparation

Cylindrical specimens of 8.8 mm in diameter and 20 mm in gauge length were manufactured and ground in the test section to achieve a smooth surface. These specimens were used to obtain the cyclic stress–strain curves and the fatigue lifetime under constant plastic strain amplitude loading for both thermal conditions, as-received and aged. As it is very difficult to observe the initiation and growth of the fatigue crack over the whole gauge section of a cylindrically uniform specimen, a slightly radiused notch was machined at the center of the specimen, (Fig. 2). The notch focuses the fatigue damage in the zone of observation, (stress concentration factor is 1.06 at the notch tip). The surface of the shallow notch was given and additional mechanical and electrolytical polish to facilitate the observation of crack nucleation and the growth of short-cracks. The central part of the notch was monitored during the test using plastic replicas.

2.3. Low cycle fatigue test conditions

The tension/compression low-cycle fatigue tests were performed at room temperature on an electromechanic testing machine INSTRON 1362. The tests were carried out under plastic strain control with a fully reversed triangular wave at constant total strain amplitude of 0.3% and total strain rate of $2 \times 10^{-3}\ s^{-1}$. After the first 300 cycles, the test was stopped each 150 cycles with the crosshead of the machine in tension (about 80% of the peak tensile stress of the cycle) to record the damage on the surface of the shallow notch. The main crack appears in the gage length at about half the fatigue life.

2.4. Crack observations

In order to monitor the evolution of the crack, the surface relief in of the shallow notch was recorded by using plastic replicas. The dried replicas were examined using an optical microscope in order to follow the failure back to the fatigue crack initiation phase. The replicated surface of the specimen was systematically explored and the images were stored to reproduce the initiation, growth

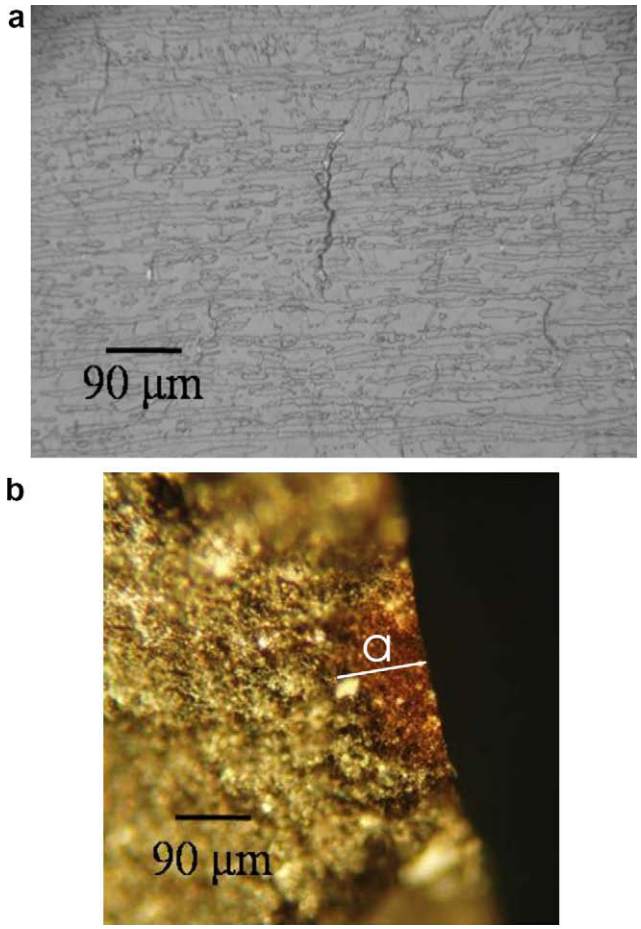

Fig. 3. (a) Image of the surface crack subjected to the heat tinting technique and (b) Image of the same crack after the heat tinting treatment.

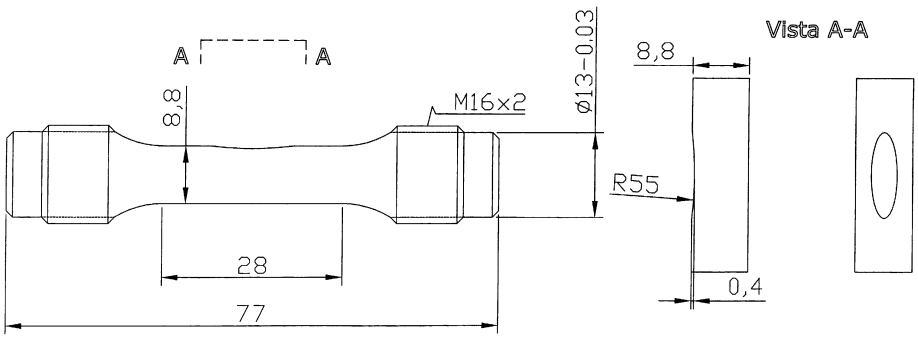

Fig. 2. Diagram of the shallow-notched specimen.

and coalescence of the microcracks. This procedure consisted of measuring the projected surface crack length on the surface line perpendicular to the specimen axis.

In a similar test, the true length of the crack advancing into the interior of the specimen, perpendicular to the tensile axis was estimated using the heat tinting method. Once the cracks projected on the shallow surface of the specimen notch had reached a length of about 200–250 μm, as measured by replicas, Fig. 3a, the specimen was heated to 450 °C for 1 h and then cooled to room temperature. Afterwards, the test was continued up to rupture. This procedure was performed in the aged specimen since the information for the as-received material was found in the literature [5]. The result of this test demonstrated that half of the projected length is equal to the semicircle radius and thus is considered as the crack length, *a*, Fig. 3b. It is interesting to point out that both, the as-received and the aged specimens give rise to a semicircular microcrack.

In the following, we will refer to a microcrack as a crack whose propagation depends on the surrounding microstructure, while a short-crack is the result of microcrack coalescence, when the microstructure is no longer important. Lastly, the term crack will be used generally but always in the context of small cracks.

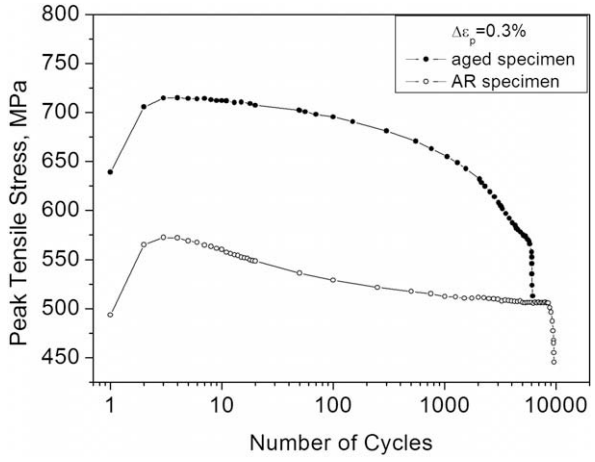

Fig. 4. Cyclic curves from the as-received and aged specimens measured on standard, smooth, cylindrical specimens subjected to constant plastic strain range loading.

2.5. Dislocation structure

Internal dislocation structures were studied in thin foils taken from slices cut at different depths, parallel to the specimen axis, from the shallow-notched area of the specimen on the side opposite the dominant crack. The foils were taken when the dominant crack was of the order of 500 μm. Thin foils were prepared with a double jet of a solution of 10% perchloric acid and ethanol, keeping the current density and temperature at 70 mA and 5 °C, respectively. Observations of dislocation structures were performed using a Transmission Electron Microscope (TEM Philips EM 300) at an accelerating voltage of 100 kV. Special care was taken to mark the direction of the specimen axis so that the orientation of each grain relative to the loading axis could be determined. Bright field imaging conditions were adopted and the diffraction patterns were used to determine the grain orientation and main crystallographic directions.

3. Results

3.1. Mechanical results

The cyclic curves measured on standard smooth cylindrical specimens subjected to constant plastic strain amplitude loading are shown in Fig. 4. The fatigue life of the aged samples is close to that of the specimens tested in the as-received conditions with an uncertainty of 30%.

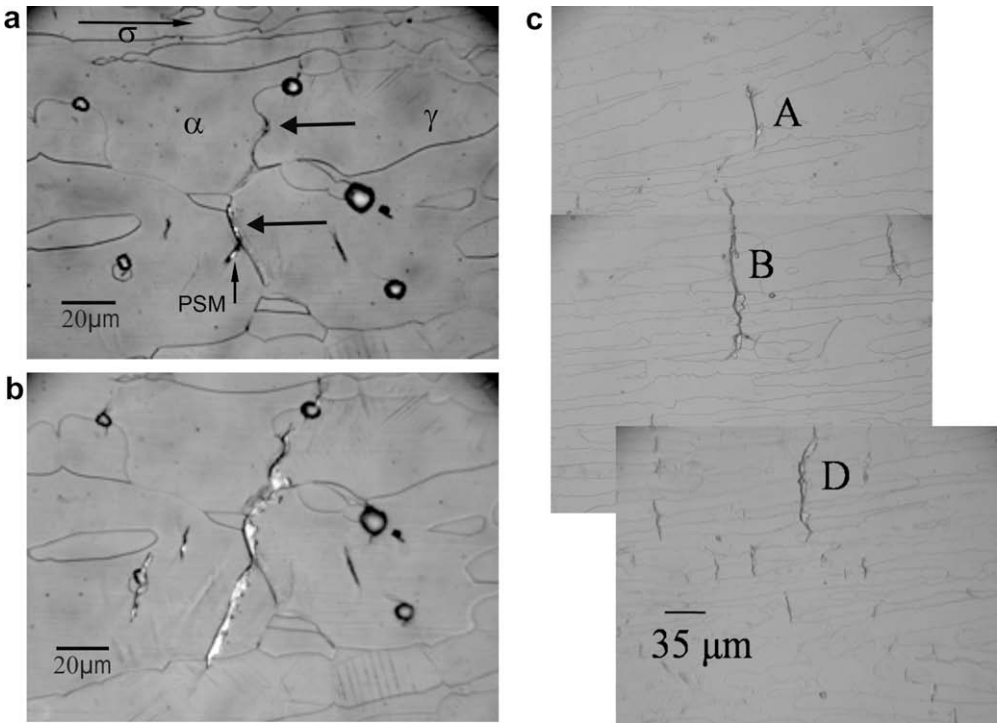

Fig. 5. Nucleation and propagation of typical microcracks in the as-received DSS: (a) damage situation at 1100 cycles, the arrows show the nucleation site of two microcracks at 450 cycles and (b) at 2150 cycles, the microcracks have coalesced and propagated along a PSM in the ferrite (see arrow).

3.1.1. Crack growth in the as-received material

The first microcracks, observed after 450 cycles, nucleated preferentially at α/α or α/γ boundaries located nearly perpendicular to the tensile stress, Fig. 5a. In this figure, the arrows show the nucleation location of two microcracks in the phase boundaries at the end of a PSM. Persistent slip markings (PSM) and other α/α or α/γ boundaries are the path of propagation of these microcracks as shown in Fig. 5b. The presence of second-phase particles also results in local stress and strain concentrations, favoring microcrack initiation.

Fig. 5c exhibits three short-cracks after 3450 cycles that will give rise to the final macrocrack at 4750 cycles. Microcracks A and B were nucleated in α/α and α/γ boundaries, respectively, and D in a second-phase particle In general, in the as-received material the crack density is very low and is concentrated in the central part of the notch where the stress and strain concentration is higher due to the geometry of the specimen. According to the new concepts of Zhao et al. [6], this zone evolves by the formation of '*effective short fatigue cracks*' *(ESFC)*, i.e. cracks that lies in the growth path of the '*dominant effective short fatigue crack*' *(DESFC)* which results in the specimen failure.

Fig. 6a shows the growth curve of the three microcracks shown in Fig. 5c, and their coalescence into the final crack (Crack 1). Similar to the result obtained by Polak and Zezulka [5], it follows an exponential behavior. Fig. 6b shows only the behavior of the microcracks below 100 μm in length. It is interesting to note that above a length of 60 μm the microstructure was no longer important for microcrack growth and the growth curve that represent the microcrack advanced follows an exponential law.

3.1.2. Crack growth in the Aged material

In the aged material, contrary to the behavior observed in the as-received material, microcracks nucleate at persistent slip markings in the ferritic phase. The microcrack density is substantially higher and their distribution more homogenous over a wider central zone of the notched specimen for an equivalent number of cycles. Fig. 7a shows the nucleation site of a microcrack at 550 cycles on a straight PSM oriented nearly at 45° from the tensile axis in the

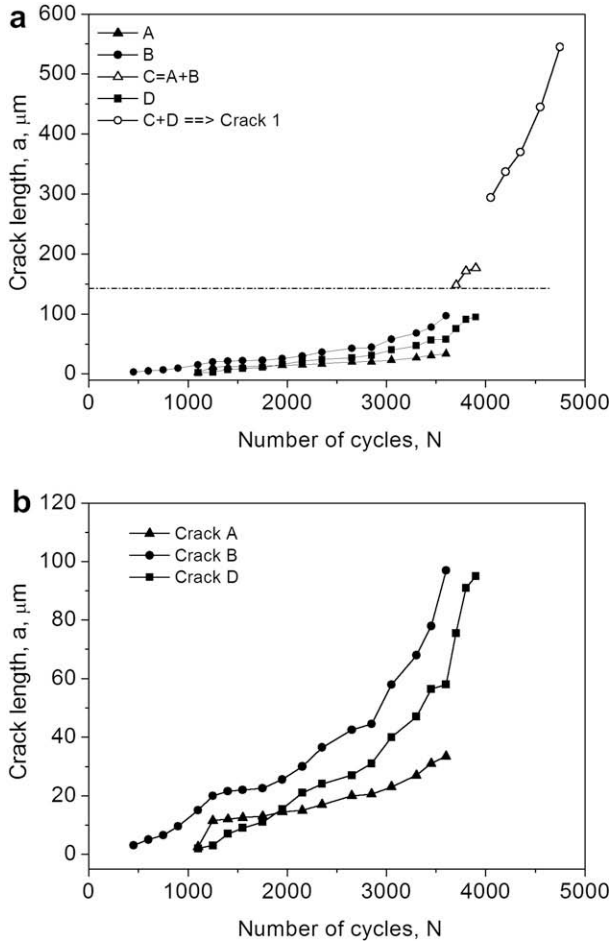

Fig. 6. (a) evolution of microcracks A, B and D and the coalescence into final Crack 1 and (b) Magnification of the growth curves before the formation of the macrocrack.

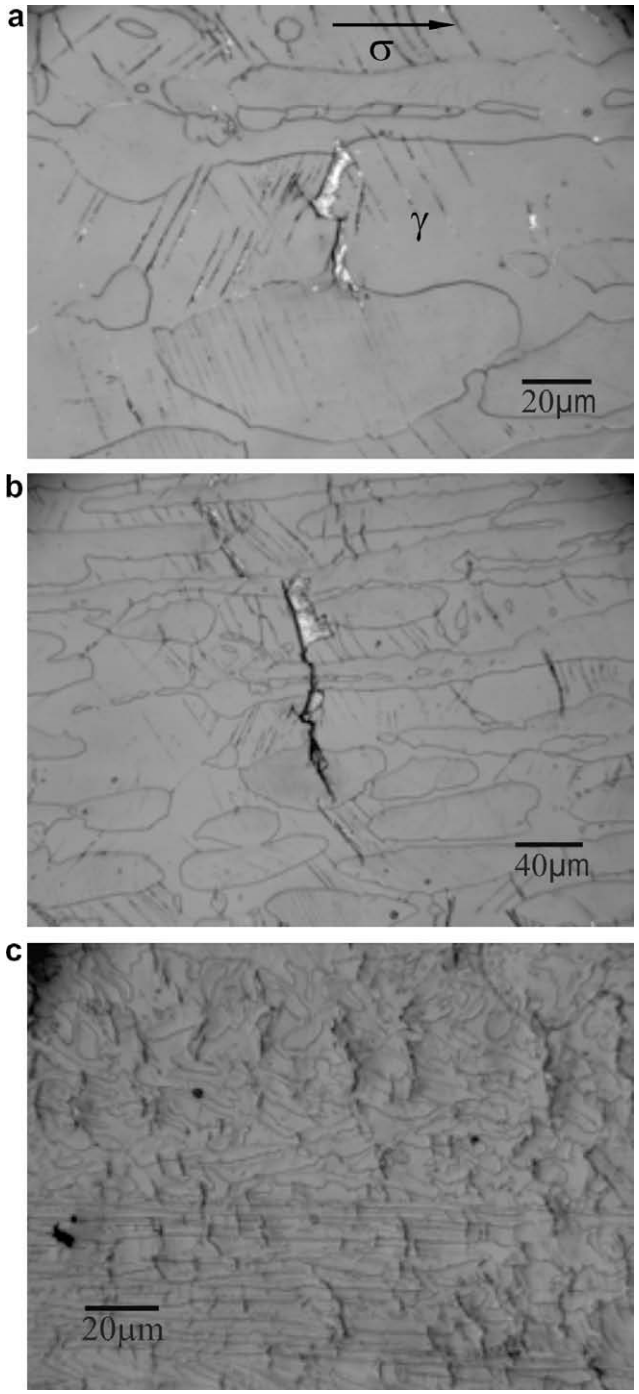

Fig. 7. (a) Nucleation site of a general microcrack on a straight PSM oriented nearly at 45° to the tensile axis in the ferritic phase (550 cycles); (b) the same area at 1350 cycles and (c) distribution and microcrack density at 2700 cycles.

ferritic phase. It is interesting to mention that slip markings form in the ferritic phase much earlier than in the austenitic phase. Then, Fig. 7b shows the propagation process of this microcrack and the nucleation of new microcracks on PSM within other ferritic grains that lie in the growth path of the first microcrack. Fig. 7c shows the distribution and density of microcrack at 2700 cycles.

Fig. 8a shows the evolution of all the microcracks that will give rise to the final dominant effective short fatigue crack, named Crack 2. The formation of this crack corresponds to the contribution of numerous microcracks well below 50 μm in length leading to the formation of the dominant crack. This observation is contrary to our observation for the as-received material.

Fig. 8b shows in more detail the individual behavior of the microcracks when they are still below 100 μm in length. All of them growth linearly with the number of cycles and at the same rate except microcrack named A. This microcrack is the only one that was nucleated in a ferritic grain with dimensions larger than the rest. In order to directly compare the microcrack growth behavior in the as-received and aged materials, we have plotted microcrack B from Fig. 6 and microcrack A from Fig. 8 both in Fig. 9. This plot exhibits several interesting features. Firstly, the growth behavior of microcrack B was analyzed through replicas and we could identify sites where the crack arrested, overcome the phase boundary and where the phase boundary was no longer an obstacle. Secondly, the growth rate of this microcrack was not constant. For lengths less than 100 μm, the microcrack accelerated and decelerated constantly, but once the crack length exceeded 150 μm (Fig. 6), the growth was exponential. On the other hand, in the aged material, the microcrack grew at constant rate and phase boundaries did not act as crystallographic barriers. The microcracks passed through these barriers without any decrease in velocity.

3.2. TEM observations

3.2.1. As-received material

The analysis of the dislocation structure developed at different depths beneath the specimen surface in the notched area for crack lengths of 500 μm has revealed interesting features. In the austenitic

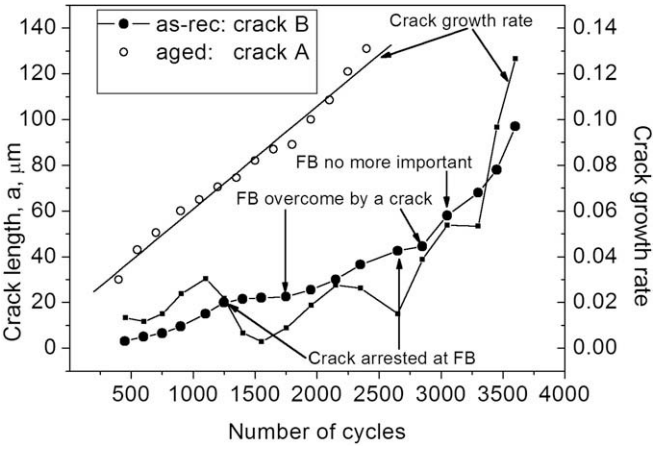

Fig. 9. Comparison of microcrak growth curves in the as-received and aged materials.

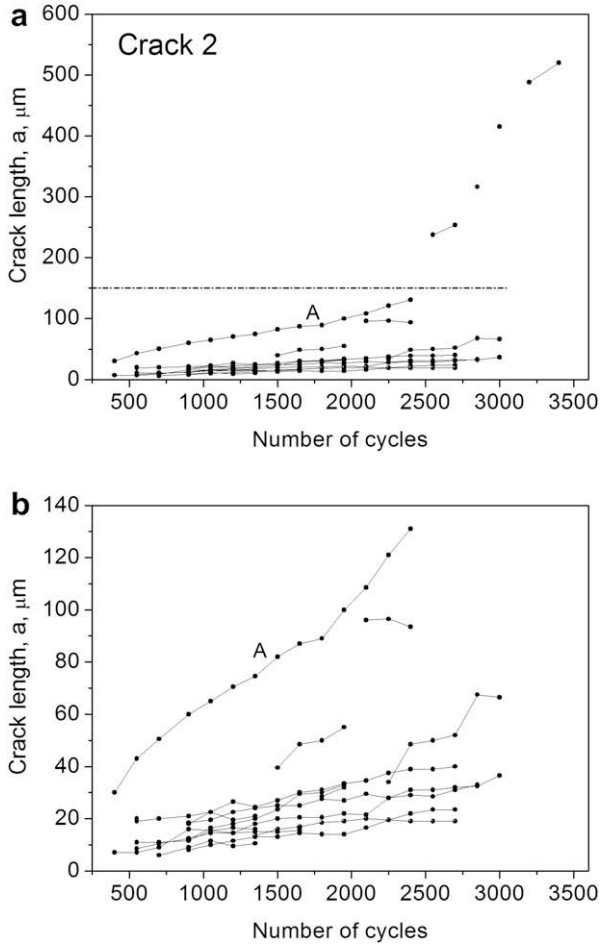

Fig. 8. (a) Evolution of microcracks and their coalescence into final Crack 2 in the aged material and (b) Magnification of the growth curves before the formation of the macrocrack.

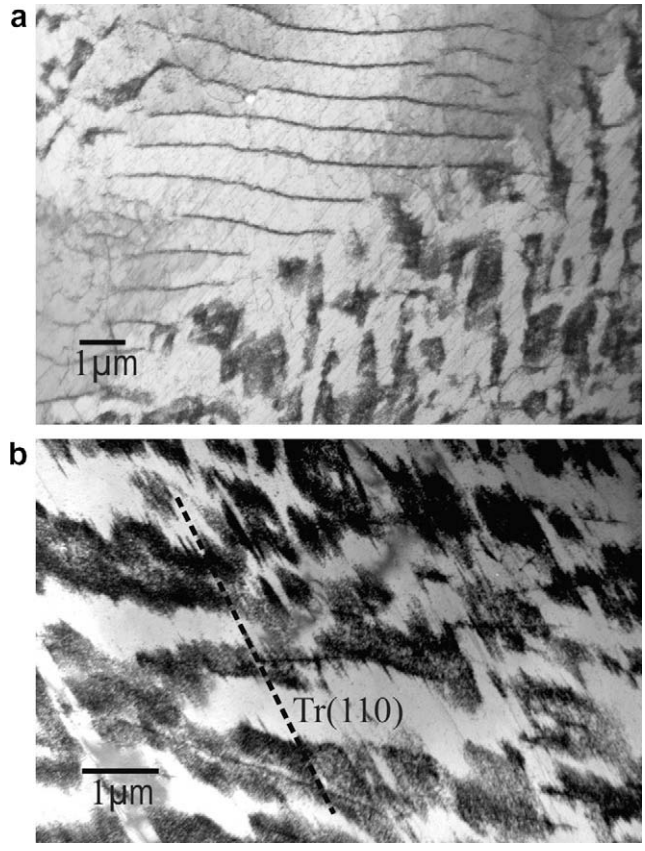

Fig. 10. (a) Typical dislocation arrangement corresponding to cyclic strain localization in ferritic grains and (b) localization of cyclic plastic strain into well-formed PSBs.

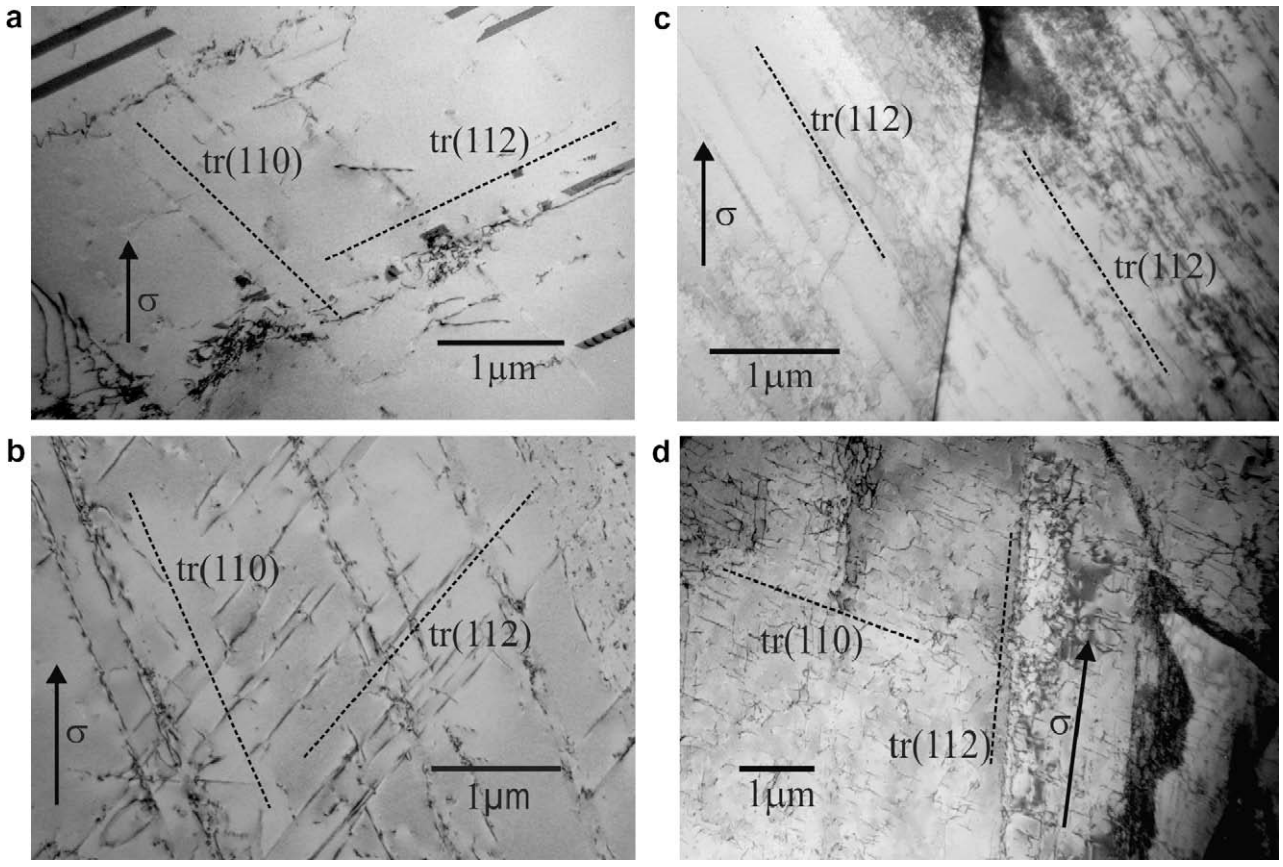

Fig. 11. Dislocation structure developed in the aged specimen (a) and (b) defining the activated deformation planes; (c) arrays of micro twins in the ferritic phase and (d) distribution of single dislocations on {1 1 0} and {1 1 2} planes and extended microtwins throughout the grain.

phase, a planar arrangement of dislocations that can reorganize into an ill-formed cell structure when the thin foils were taken close to the notch surface while the ferritic grains formed a well-defined vein structure independent of the slice depth from which the thin foils were taken. However, the dislocation structure responsible for cyclic strain localization is different to that of veins. Fig. 10a, from a foil taken 5.3 mm beneath the specimen surface, shows a typical dislocation arrangement corresponding to the localization of cyclic plastic strain. In the micrograph, the vein structure has rearranged into alternating walls and channels. That is, thin dislocation-rich regions, walls, and wide dislocation-poor zones, channels. Taken from a region where deformation is more localized, Fig. 10b shows a typical example of the dislocation arrangement corresponding to the localization of cyclic plastic strain into persistent slip bands (PSB). A similar structure was observed either close (1 mm) or far away (5.3 mm) from the specimen surface. The characteristic "ladder-like structure" is similar to that seen in other materials [7]. It corresponds to various thin sheets of alternating walls and channels of different thickness, immersed in a clearly distinctive surrounding matrix structure. The structure of PSB lamellae lying parallel to the primary slip plane (1 1 0) is oriented at nearly 45° to the tensile axis.

3.2.2. Aged material

A planar arrangement of dislocations not showing distinctive features developed in the austenitic phase during cycling on the aged material. However, when the thin foils are taken from discs close to the notch surface, an ill-formed cell structure could be observed. This structure is similar to what was observed in the austenite of the as-received material. On the other hand, in the aged material, the dislocation structure in the ferrite is completely different from that of the as-received material. The aged ferritic structure also depends on the depth from which the thin foils were taken. Fig. 11a and b show that cycling activated several slip modes in the ferritic phase of the aged specimen. Fig. 11a shows the activation of a {1 1 0} slip plane of unit dislocations and a {1 1 2} slip plane of dissociated dislocations oriented at about 45° and 60° from the tensile axis, respectively. This result is consistent with those made by optical microscopy of replicas for example Fig. 7a in which two well-defined slip directions are observed. It is important to draw attention to the planar nature of the dislocations on the {1 1 0} planes. Under certain conditions, i.e. temperature, alloying elements, etc, glide dislocations in iron tend to be restricted to a specific slip plane. A possible, but unsubstantiated, explanation of these observations in the aged matrix is that the unit dislocation is either dissociated into partials or has an asymmetrical core structure which restricts the free movement of the screw dislocations. In Fig. 11b, the situation is similar but in this case microtwins have nucleated on the traces of the {1 1 2} planes. Generally, arrays of microtwins, Fig. 11c, were observed in ferritic grains near the free surface of the notch (about 1mm below the surface). Far away from the surface, Fig 11d, the microstructure consists of a distribution of single dislocations on {1 1 0} and {1 1 2} planes and extended microtwins throughout the grain that can even lie nearly aligned with the tensile axis.

4. Discussion and conclusions

The preferred sites for the initiation of the fatigue microcracks in the austenitic-ferritic duplex stainless steel in the as-received condition cyclically loaded over a 0.3% plastic strain range are mainly α/α or α/γ boundaries that are located nearly perpendicular to the tensile stress. The microcrack propagation path is generally

along slip markings in ferritic or austenitic grains and other α/α or α/γ boundaries. Similar results have been reported by El Bartali et al. [8] who analyzed surface damage with a digital image correlation technique in the X2 Cr Ni Mo 25-07 DSS. Contrary to our results, they observed intense strain localization zones in some places from the first cycles and microcrack initiations that correlated with some of these high strain-gradient zones. The fact that the first microcracks nucleate at phase or grain boundaries can be rationalized by analyzing the dislocation structure and the structure associated with strain localization. The dislocation structure in the ferritic grains, which was independent of the depth from which the thin foils were taken, develops a well-formed PSB, oriented nearly 45° from the tensile axis, embedded in the matrix structure. The interface between the PSB and matrix is a plane of discontinuity across which there are abrupt gradients in the density and dislocation distribution. Thus, these interfaces serve as preferential sites for fatigue crack nucleation in free surface grains. In interior grains, the formation of a PSB is associated with grain-boundary stress concentrations that would assist crack nucleation [9].

In aged specimens, the nucleation and distribution of microcracks as well as the microstructure developed in ferritic grains are completely different in comparison to the as-received material. This enormous difference in the behavior of microcrack nucleation can be attributed to the change in deformation mode observed in the ferritic phase of the aged material due to the spinodal decomposition. Ageing ferritic steels at 475 °C leads to the spinodal decomposition into Fe-rich (α) and Cr-rich (α'). The deformation by dislocation slip is reduced in the spinodal decomposed ferrite and increases the deformation by twinning. This change in the plasticity causes fracture by cleavage in ferritic steels [4].

In the as-received material strain localization is the result of PSB nucleation in the hard matrix structure on {1 1 0} planes after a large strain accumulation [10]. On the other hand, in the aged material the formation of slip markings on the ferritic phase starts practically from the beginning of cycling and is the result of the deformation by gliding on {1 1 0} planes and by twining on {1 1 2} planes.

During the development of mechanical twins, thin lamellae appear very quickly and these thicken with increasing stress. The shear process involved in twining must occur by the movement of partial dislocations and, thus, the stress to cause twining will depend not only on the line tension of the source dislocation, as in the case of slip, but also on the surface tension of the twin boundary. The stress to cause twining is, therefore, usually greater than that required for slip. As the aged matrix is harder than that of the as-received material, as was stated in Section 2.1, the critical shear stress for slip increases and then, because the general stress level will be high, the process of deformation twinning is more likely. Once formed, the twin can propagate provided the resolved shear stress is higher than a critical value. Typically, this value is much lower than that for nucleation. One possible mechanism [11] to nucleate twins in bcc metals is the development of a stress concentration at the head of a piled-up array of dislocations produced by burst of slip. This is the same manner in which a Frank-Read source operates. Generally, such behavior is favored by impact loading but at normal strain rates, it should be easier to produce slip burst suitable for twin nucleation in a material with strongly locked dislocations as is the case of the present aged ferritic phase.

Twins, once formed, may themselves act as barriers like grain boundaries. The simplest mechanism whereby glide dislocations are converted into cracks is that involving a pile-up of dislocations against twin interfaces. The applied stress pushes the dislocations together, and a crack forms beneath their coalesced half-planes. This could explain the sudden formation of a high density of microcracks nucleated on slip markings over the entire strained area of the notched specimen, as observed in Fig. 7c. Although the propagation of microcracks, through the collective process of microcrack coalescence on neighbor ferritic phases following the path of the DESFC has been observed, the analysis in relation to the adjacent austenitic grains is still being evaluated.

In previous work related to short-crack propagation in as-received duplex stainless steel [12], it was observed that microcracking usually initiates in α/α grain boundaries, propagates along slip markings and is able to cross phases without delay if the Kurdjumov–Sachs K–S crystallographic relations are satisfied. When the K–S relation ship between phases is not satisfying, the crack arrested at the phase boundary. Only when the area between the traces on the grain-boundary plane is fractured the crack propagation reinitiate moving across the boundary as it was proposed by Zhai [13]. Nevertheless, in the aged material, microcracks nucleate on {1 1 2} twining planes, which are not crystallographically correlated between phases as occurs between $\{1\,1\,0\}_\alpha$ and $\{1\,1\,1\}_\gamma$ planes in the K–S relationship. Therefore, one would expect that the microcracks should remain arrested at a phase boundary until the crack on the grain-boundary plane is produced. However, the growth rate data in Fig. 9 clearly show that microcracks in the ferritic grains do not arrest at phase boundaries like occurs in the as-received material. It is not yet clear why this is the case, and it is subject of continuing research.

Regarding microcrack growth, below a length of 100 μm, the surrounding microstructure controls the rate of microcrack advance, following different laws for the as-received and aged conditions. For the as-received materials, growth follows an exponential law, beginning slowly and rapidly accelerating as shown in Fig. 9. Meanwhile, in the aged material, the growth behaves linearly. In this case a large number of microcracks grow collectively in grains located in the *growth path of the dominant crack,* contributing to the same final crack.

In summary, the factor that controls the nucleation and growth of a microcrack in the as-received material is the generation of PSBs, which form sites of microcrack nucleation at grain boundaries and provide paths for microcrack propagation. After the crack length reaches 100 μm, the microstructure is no longer important and the law of propagation is ruled by mechanical parameters. In the aged material, microcracks first initiate in the ferritic phase because of a sudden nucleation of microtwins on {1 1 2} planes. The twinning is driven by high applied stresses which are a consequence of a hardened ferritic matrix. In addition, the growth rate is constant and phase boundaries do not provide major resistance to the propagation of the microcracks.

Acknowledgements

This work was supported by the Agencia Nacional para la Promoción de la Ciencia y Técnica (ANPCYT), the Consejo Nacional de Investigaciones Científicas y Técnicas (CONICET) of Argentine and by the cooperation program ECOS-Sud/SECyT between France and Argentina (Code A06E01).

References

[1] Gunn RN. Duplex Stainless Steels. Cambridge: Abington; 1997.
[2] Armas AF, Degallaix S, Degallaix G, Hereñú S, Marinelli MC, Alvarez-Armas I. Beneficial effects induced by high temperature cycling in aged duplex stainless steel. Key Eng Mater 2007;345/346:339–42.
[3] Armas AF, Hereñú S, Alvarez-Armas I, Degallaix S, Condó A, Lovey F. The influence of temperature on the cyclic behavior of aged and unaged super duplex stainless steels. Mater Sci Eng A 2008;491:434–9.
[4] Bugat S, Besson J, Gourgues A-F, N'Guyen F, Pineau A. Mater Sci Eng 2001;A317:32–6.
[5] Polak J, Zezulka P. Short crack growth and fatigue life in austenitic-ferritic duplex stainless steel. Fatigue Fract Eng Mater Struct 2005;28:923–35.
[6] Zhao YX, Gao Q, Wang JN. Interaction and evolution of short fatigue cracks. Fatigue Fract Eng Mater Struct 1999;22:459–67.

[7] Lukas M, Kesnil P. Fatigue of metallic materials MSM, 7. Elsevier; 1980.
[8] El Bartali A, Aubin V, Degallaix S. Fatigue damage analysis in a duplex stainless steel by digital image correlation technique. Fatigue Fract Eng Mater Struct 2008;31:137–51.
[9] Essmann U, Gösele U, Mughrabi H. A model of extrusions and intrusions in fatigued metals-I. Point-defect production and the growth of extrusions. Phil Mag A 1981;44:405–26.
[10] Suresh S. Fatigue of materials. second ed. Cambridge University Press; 1998.
[11] Hull D. Introduction to dislocations. Pergamon Press; 1975.
[12] Marinelli MC, El Bartali A, Signorelli JW, Evrard P, Aubin V, Alvarez-Armas I, Degallaix-Moreuil S. Activated slip systems and microcrack path in LCF of a duplex stainless steel. Mat Sci Eng A 2009, in press.
[13] Zhai T, Wilkinson AJ, Martin JW. A crystallographic mechanism for fatigue crack propagation through grain boundaries. Acta mater 2000;48:4917–27.